Unusual Conductivity Patterns in Reduced Mesoporous Titanium, Niobium, and Tantalum Oxides with One-Dimensional Potassium Fulleride Wires in the Channels

Bing Ye,[†] Michel Trudeau,[‡] and David Antonelli*,[†]

Department of Chemistry and Biochemistry, The University of Windsor, 401 Sunset Avenue, Windsor, Ontario N9B-3P4, Canada, and Emerging Technologies, Hydro-Québec Research Institute, 1800 Boulevard Lionel-Boulet, Varennes, Quebec, J3X 1S1, Canada

Received May 2, 2001. Revised Manuscript Received June 5, 2001

Recent results in our group demonstrated that K_nC_{60} ($n = 3$), a much-studied superconductor and molecular metal, can be encapsulated in the channels of mesoporous niobium oxide to make pseudo-one-dimensional alkali fulleride wires. The oxidation state of the encapsulated fulleride phase can be tuned by addition of potassium naphthalene to the mesostructured composite. Surprisingly, the conductivity of this series of composites has maxima at $n = 2.6$ and $n = 4.1$, rather than $n = 3$ as in the bulk material. In this work, we report a study on the effect of changing the pore size and wall composition of the mesoporous host lattice on the conductivity and electronic behavior of the corresponding potassium fulleride composites. Samples of mesoporous niobium oxide with a 32-Å pore size, mesoporous tantalum oxide with a 22-Å pore size, and mesoporous titanium oxide with a 22-Å pore size were treated with K_3C_{60} and characterized by elemental analysis, nitrogen adsorption, X-ray diffraction (XRD), Raman spectroscopy, X-ray photoelectron spectroscopy (XPS), electron spin resonance spectroscopy (ESR), and superconducting quantum interference device (SQUID) magnetometry. These materials were then further reduced with small aliquots of potassium naphthalene in sequential steps up to a fulleride oxidation state of $n = 4.5$, and each material was fully characterized as described above. For each series of materials, two conductivity maxima were observed, the first at approximately $n = 2.5$ and the second at roughly $n = 4.0$, indicating that this double-maxima behavior is general to other one-dimensional alkali fulleride mesostructures. There was no clear pattern in the effect of changing pore size and wall composition on the electronic properties; however, all materials near $n = 4.0$ showed a greater degree of reduction of the mesostructure and a greater density of states near the Fermi level as determined by XPS, consistent with the high levels of conductivity of the fulleride at this oxidation state.

Introduction

The fabrication of organic−inorganic materials with periodic structural features on the nanoscale is one of the most active areas of current materials research.[1] Composite materials can now be designed to adopt the structural imprint of an organic micelle[2−7] or polymer phase,[8,9] allowing levels of shape and porosity control hitherto not possible.[10] Despite these recent advances, the fabrication of electronic and magnetic properties into such shape-controlled organic−inorganic composites still represents a frontier in materials research. Advances in this area will lead to materials with highly unusual physical behavior because of cooperative behavior between regions of very different structural, magnetic, and electronic properties. Incorporation of carbon nanotubes,[11] photosensitive light-harvesting complexes,[12] and molecules with nonlinear optical properties[13] into inorganic frameworks with periodic structures can lead to materials with properties not possessed by either the pure organic or the pure inorganic phase.

* Author to whom correspondence should be addressed.
[†] The University of Windsor.
[‡] Hydro-Québec Research Institute.

(1) Ball, P. *Made to Measure*; Princeton University Press: Princeton, NJ, 1997.
(2) Kresge, C. T.; Leonowicz, M. E. Roth, W. J.; Vartulli, J. C.; Beck, J. S. *Nature* **1992**, *359*, 710.
(3) Huo, Q.; Margolese, D. I.; Ciesla, U.; Demuth, D. G.; Feng, P. Gier, T. E.; Sieger, P.; Firouzi, A.; Chmelka, B. F.; Schuth, F.; Stucky, G. D. *Chem. Mater.* **1994**, *6*, 1176.
(4) Chen, C.-Y.; Burkette, S. L.; Li, H.-X.; Davis, M. E. *Microporous Mater.* **1993**, *2*, 27.
(5) Tanev, P. T.; Chibwe, M.; Pinnavaia, T. J. *Nature* **1994**, *368*, 321.
(6) P. Behrens, P. *Angew. Chem., Int. Ed. Engl.* **1996**, *35*, 515.
(7) Antonelli, D. M.; Ying, J. Y. *Curr. Opin. Colloid Interface Sci.* **1996**, *1*, 523.
(8) Antonietti, M.; Berton, B.; Goeltner, C.; Hentze, H. *Adv. Mater.* **1998**, *10* (2), 154−159.
(9) Zhao, D.; Feng, J.; Huo, Q.; Melosh, N.; Frederickson, G. H.; Chmelka, B. F.; Stucky, G. D. *Science* **1998**, *279*, 548−552.
(10) Yang, H.; Coombs, N.; Ozin, G. A. *Nature* **1997**, *386*, 692−695.
(11) Jin, Z.; Sun, X.; Xu, G.; Goh, S. H.; Ji, W. *Chem. Phys. Lett.* **2000**, *318* (6), 505−510.
(12) Cassagneau, T.; Fendler, J. H.; Johnson, S. A.; Mallouk, T. E. *Adv. Mater.* **2000**, *12*, 1363−1366.
(13) Kajzar, F.; Okada-Shudo, Y.; Merritt, C.; Kafafi, Z. *Synth. Met.* **1998**, *94*, 91−98.

10.1021/cm0104001 CCC: $20.00
Published on Web 07/17/2001

Recent advances in our group have demonstrated that mesoporous transition metal oxides[14−19] can act as potent electron acceptors,[20,21] a property not exhibited by their silica analogues. This feature allows for the coupling of host−guest inclusion reactions[22] with electron-transfer processes, allowing quantum confinement effects and nonstoichiometry to be achieved simultaneously in the guest phase. Whereas reaction of mesoporous niobium oxide with alkali metals leads to insulating reduced mesostructures with potential applications in batteries requiring fast ion conduction,[20,21] inclusion of more weakly reducing organometallic sandwich complexes into the host matrix leads to the formation of mixed-oxidation-state organometallic phases with either metallic,[23,24] superparamagnetic,[25,26] or spin-glass[27] behavior. A particularly interesting class of these composites involves one-dimensional potassium fulleride phases in the pores of mesoporous niobium oxide.[28,29] These materials are of special interest because the reason for the superconducting and metallic behavior of K_3C_{60} and related materials is not fully understood, the role of the fulleride oxidation state in the physical behavior being an area of some amount of controversy.[30,39] One unique aspect of these new mesoporous niobium oxide−potassium fulleride composites is the ease in which the oxidation state of the fulleride phase can be tuned by addition of excess potassium, thus making it possible to undertake a systematic study of the relation of composition to conductivity and low-temperature magnetic properties. Studies to date have led to the following interesting observations. First, the $n = 3$ state, most closely linked to metallic and superconducting behavior in bulk fullerides, is one of the least conducting phases in our materials, supporting calculations that this state is inherently insulating because of its half-filled conduction band. Second, the conductivity maxima are at $n = 2.6$ and $n = 4.1$ and above, with the latter materials having conductivities matching or exceeding those of many pure-phase molecular metals. Whereas the maximum at 2.6 can be related to $n = 3$ in bulk materials, the maximum at and above 4.1 has no obvious relationship to bulk fullerides, as K_4C_{60} is insulating. This suggests that some transition to a cooperative electronic state has occurred at or around the $n = 4.1$ state and that the materials at this level of reduction are best not viewed as electronically isolated fulleride nanowires in an insulating host matrix. The electronic properties depend on many factors, including the fulleride loading and oxidation state, as well as the absolute K level; however, the role of the morphology and composition of the host matrix is not yet known. Hence, to more fully understand the unusual properties of this family of materials, we present a study of the effects of the variation of pore size and wall composition of the host material on the conductivity patterns of the corresponding alkali fulleride composites.

Experimental Section

Materials and Equipment. All chemicals, unless otherwise stated, were obtained from Aldrich. Samples of mesoporous niobium oxide (Nb-TMS1) were obtained from Alfa-Aesar and used without further purification. Trimethylsilyl chloride was obtained from Aldrich and distilled over calcium hydride. M-TMS1 (M = Nb, Ta, Ti) samples were dried at 100 °C overnight under vacuum and then stirred with excess trimethylsilyl chloride in dry ether for 12 h under nitrogen. Nitrogen adsorption and desorption data were collected on a Micromeritics ASAP 2010 instrument. X-ray diffraction (XRD) patterns (Cu Kα) were recorded in a sealed glass capillary on a Siemens D-500 $\theta-2\theta$ diffractometer. All X-ray photoelectron spectroscopy (XPS) peaks were referenced to the carbon C−(C,H) peak at 284.8 eV, and the data were obtained using a Physical Electronics PHI-5500 spectrometer using charge neutralization. The conductivity measurements were recorded on a Jandel four-point universal probe head combined with a Jandel resistivity unit. The equations used for calculating the resistivity were as follows:

$$\text{for pellets of } <0.1 \text{ mm thickness} \quad \rho = \left(\frac{\pi}{\log n^2}\frac{V}{I}\right)t$$

$$\text{for pellets of } >0.5 \text{ mm thickness} \quad \rho = 2\pi(S)\left(\frac{V}{I}\right)$$

where ρ is the resistivity, $\pi/(\log n^2)$ is the sheet resistivity, V is the voltage, I is the current, t is the thickness of the pellet, and S is the the spacing of the probes (0.1 cm).

Magnetic measurements were conducted on a Quantum Design superconducting quantum interference device (SQUID) magnetometer MPMS system with a 5-T magnet. Electron spin resonance (ESR) measurements were performed on a Bruker 300E system at 9.79 GHz. The Raman spectra were recorded on a Renishaw Ramascope using a Renishaw 780-nm diode laser system. All elemental analysis data were collected under

(14) (a)Antonelli, D. M.; Ying, J. Y. *Angew. Chem., Int. Ed. Engl.* **1996**, *35*, 426. (b) Antonelli, D. M.; Ying, J. Y. *Angew. Chem., Int. Ed. Engl.* **1995**, *34*, 2014. (c) Antonelli, D. M.; Ying, J. Y. *Inorg. Chem.* **1996**, *35* (11), 3126−3136. (d) Antonelli, D. M.; Ying, J. Y. *Chem. Mater.* **1996**, *8* (4), 874−881.
(15) Reddy, J. S.; Sayari, A. *Catal. Lett.* **1996**, *38*, 219.
(16) (a) Antonelli, D. M. *Adv. Mater.* **1999**, *11*, 487. (b) Antonelli, D. M. *Microporous Mesoporous Mater.* **1999**, *30*, 315−319. (c) Antonelli, D. M. *Microporous Mesoporous Mater.* **1999**, *33*, 209−214.
(17) Tian, Z. R.; Wang, J. Y.; Duan, N. G.; Krishnan, V. V.; Suib, S. L. *Science* **1997**, *276*, 926.
(18) Antonelli, D. M.; Trudeau, M. *Angew. Chem., Int. Ed. Engl.* **1999**, *38*, 1471.
(19) Ciesla, U.; Schacht, S.; Stucky, G. D.; Unger, K.; Schüth, F. *Angew. Chem., Int. Ed. Engl.* **1996**, *35*, 541.
(20) Vettraino. M.; Trudeau, M.; Antonelli, D. M. *Adv. Mater.* **2000**, *12*, 337.
(21) Vettraino, M.; Trudeau, M.; Antonelli, D. M. *Inorg. Chem.* **2001**, *40*, 2088.
(22) Moller, K.; Bein, T. *Chem. Mater.* **1998**, *10*, 2950.
(23) He, X.; Trudeau, M.; Antonelli, D. M. *Adv. Mater.* **2000**, *12*, 1036.
(24) He, X.; Trudeau, M.; Antonelli, D. M., manuscript submitted.
(25) Murrray, S.; Trudeau, M.; Antonelli, D. M. *Adv. Mater.*, in press.
(26) Murray, S.; Trudeau, M.; Antonelli, D. M. *Inorg. Chem.* **2000**, *39*, 5901−5908.
(27) Vettraino, M.; Trudeau, M.; Antonelli, D. M. *J. Mater. Chem.* **2001**, *11*, 1−6.
(28) Ye, B.; Trudeau, M.; Antonelli, D. M. *Adv. Mater.* **2000**, *13*, 29−33.
(29) Ye, B.; Trudeau, M.; Antonelli, D. M. *Adv. Mater.* **2001**, *13*, 561.
(30) Kroto, H. W.; Heath, J. R.; O'Brien, S. C.; Curl, R. F.; Smalley, R. E. *Nature* **1985**, *318*, 162.
(31) Hebard, A. F.; Rosseinsky, M. J.; Haddon, R. C.; Murphy, D. W.; Glarum, S. H.; Palstra, T. T. M.; Ramirez, A. P.; Kortan, A. R. *Nature* **1991**, *350*, 600.
(32) Benning, P. J.; Martins, J. L.; Weaver, J. H.; Chibante, L. P. F.; Smalley, R. E. *Science* **1991**, *252*, 1417.
(33) Chakraverty, S.; Gelfand, M. P.; Kivelson S. *Science* **1991**, *254*, 970.
(34) Bezryadin, A.; Lau, C. N.; Tinkham, M. *Nature* **2000**, *404*, 971.
(35) Zaikin, A. D.; Golubev, D. S.; Van Otterlo, A.; Zimanyi, G. T. *Phys. Rev. Lett.* **1997**, *78*, 1552.
(36) Kosaka, M.; Tanigaki, K.; Prassides, K.; Margedonna, S.; Lappas, A.; Brown, C. M.; Fitch, A. N. *Phys. Rev.* **1999**, *59*, 6628.
(37) Lof, R. W.; van Veenendaal, M. A.; Koopmans, B.; Jonkman, H. T.; Sawatzky, G. A. *Phys. Rev. Lett.* **1992**, *68*, 3924.
(38) Yildrium, T.; Barbedette, L.; Fischer, J. E.; Lin, C. L.; Robert, J.; Petit, P.; Palstra, T. T. M. *Phys. Rev. Lett.* **1996**, *77*, 167.
(39) Pichler, T.; Matus, M.; Kürti, J.; Kuzmany, H. *Phys. Rev. B* **1992**, *45*, 13841.

an inert atmosphere by Galbraith Laboratories, 2323 Sycamore Drive, Knoxville, TN 37921-1700. Metal analysis was conducted by inductively coupled plasma (ICP) techniques.

Synthesis. To a suspension of the M-TMS1 (M = Nb, Ta, Ti) in dry THF was added excess K_3C_{60} (synthesized by heating C_{60} and K together in a sealed tube at 200−400 °C and then characterized by XRD), as calculated on the basis of %M determined from the elemental analysis data. The mesoporous solid immediately changed from a light tan color to a deep gray-black (Nb-TMS1). After several days and additional stirring to ensure complete absorption of the fulleride, the reduced material was collected by suction filtration and washed several times with THF. Once synthesized, the material was dried in vacuo at 10^{-3} Torr on a Schlenk line until all condensable volatiles had been removed. This procedure is normally sufficient to remove any solvent molecules from the fulleride phase. Further reduction of these materials was accomplished by addition of a predetermined quantity (calculated on the basis of the percentage of C_{60} in the material) of a stock solution of potassium naphthalene in THF to a stirred solution of the composite in THF. After being stirred overnight, the material was collected by suction filtration and washed several times with benzene until the washings were colorless. The material was then dried in vacuo at 10^{-3} Torr on a Schlenk line until all condensable volatiles had been removed. All materials were characterized by Raman spectroscopy, XPS, and elemental analysis to ensure sample quality before proceeding with SQUID and EPR characterizations. Conductivity studies were conducted in triplicate in an inert atmosphere, with the system allowed to stabilize for 30 min for each reading to ensure reproducibility.

Results and Discussion

Large-Pore Nb Materials. To investigate the effect of increased pore size on the conductivity of mesoporous niobium oxide composites of potassium fullerides a sample of mesoporous niobium oxide with a pore size of 32 Å was prepared and treated with K_3C_{60}. We reasoned that larger pores not only would attenuate any pore constriction effects, which could lead to discontinuities in the fulleride phase and a drop in bulk conductivity, but would also allow the fulleride units to span two or more unit-cell lengths (ca. 14 Å) across the channel rather than one, allowing for an increase in the dimensionality of the intercalated phase. This would lead to electronic properties more closely resembling those of bulk fullerides, as physical behavior is highly dependent on the dimensions of the material in question. Further, because one-dimensional materials often undergo lattice distortions that can dramatically alter conductivity,[40] allowing the fulleride units to span more than one unit cell-length across the pore diameter would tend to suppress any of these effects, which normally lead to charge density waves and electron localization in the channels of the material.

Titration of a trimethylsilated sample of mesoporous niobium oxide (Nb-TMS1) having an HK (Horvath−Kawazoe) pore size of 32 Å, a BET (Brunauer−Emmet−Teller) surface area of 638 m^2/g, and an XRD peak centered at $d = 44$ Å with aliquots of K_3C_{60} in THF over 1 week until maximum absorption is achieved leads to a new black solid exhibiting a strong X-ray powder diffraction (XRD) peak centered at $d = 44$ Å (Figure 1a), virtually the same as that obtained from the starting material. There were no other peaks at higher angles, suggesting that there is no long-range order in the fulleride phase of the material. The BET surface area of this new material dropped from 638 to 217 m^2/g (Figure 2a), and the HK pore size fell from 32 to less than 17 Å. The cumulative desorption pore volume of this sample also showed a decrease to 0.170 from 0.353 cm^3/g in the starting material. These data are consistent with absorption of a large amount of the fulleride salt into the mesopores of the material. Elemental analysis (Table 1) gave values of 45.64% C and 7.14% K with a K:C_{60} ratio of 3.0:1.0, assuming that all of the carbon in this material in excess of the 1.28% present in the starting material was due to absorbed fulleride. The carbon content in this material is greater than that in

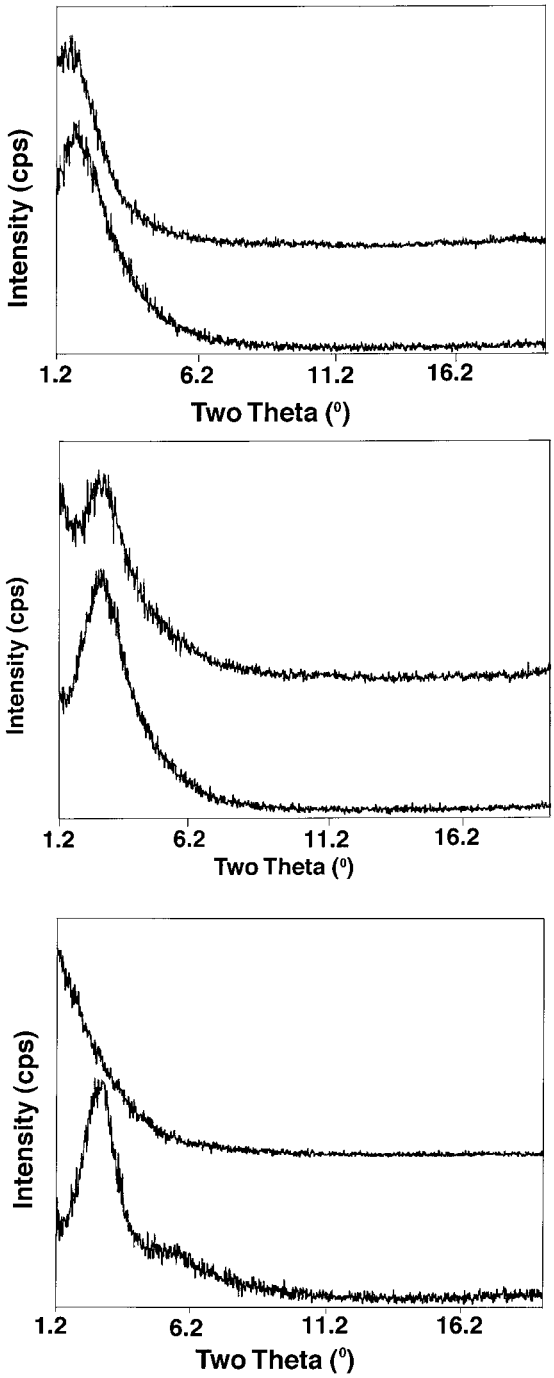

Figure 1. X-ray powder pattern of samples of (a) large-pore mesoporous niobium oxide, (b) mesoporous tantalum oxide, and (c) mesoporous titanium oxide before (lower) and after (upper) treatment with excess K_3C_{60} in THF.

(40) Williams, J. M. *Prog. Inorg. Chem.* **1985**, *33*, 183.

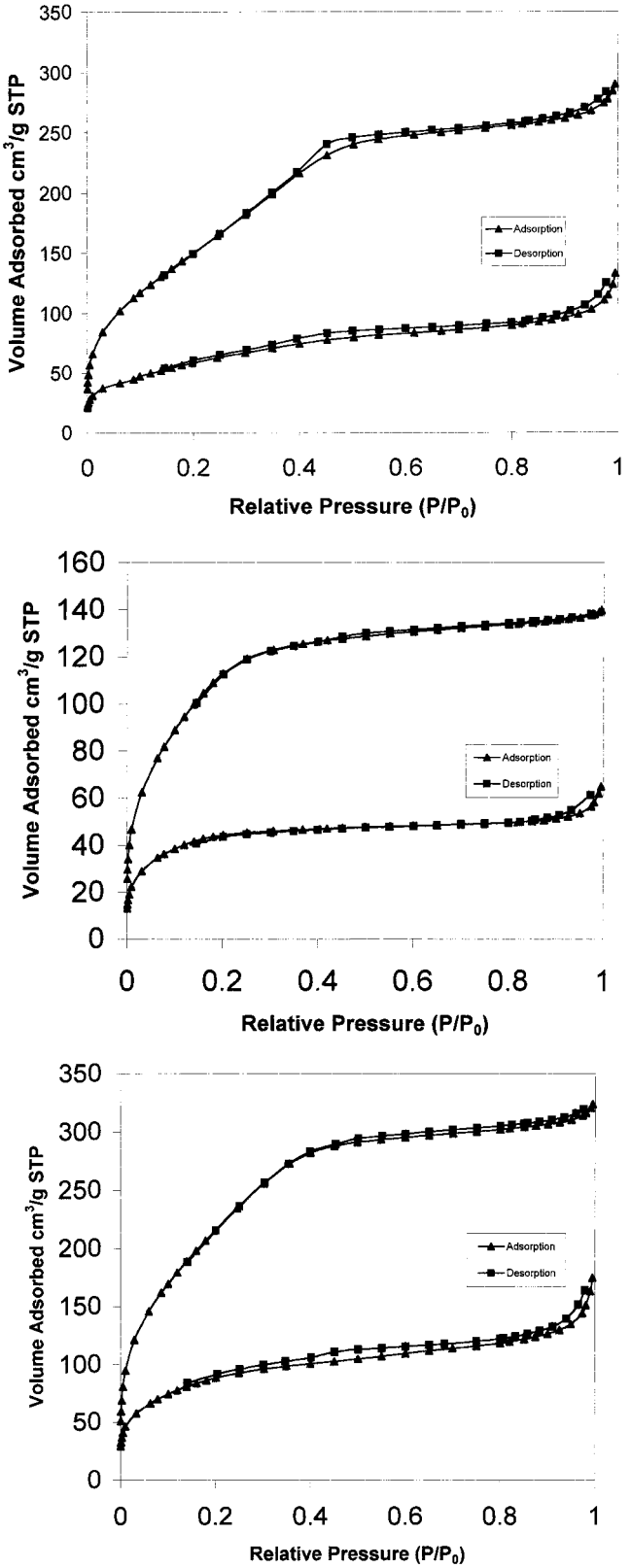

Figure 2. Nitrogen adsorption and desorption isotherms for samples of (a) large-pore mesoporous niobium oxide, (b) mesoporous tantalum oxide, and (c) mesoporous titanium oxide before (upper) and after (lower) treatment with K_3C_{60}. The loss of surface area and decreased pore volumes are consistent with filling of the pores with individual K_3C_{60} units (a = 14 Å).

the smaller-pore Nb material (29.88%) previously studied, possibly because the larger pore size allows more facile diffusion of the fulleride into the channels and,

Table 1. Table of Elemental Analysis Values for Samples of Mesoporous Oxides Intercalated with Potassium Fulleride at Various Levels of Reduction

sample ID[a]	carbon %	potassium %	molar ratio (C_{60}:K)
Nb(0.5)	45.64	7.14	1:3.0
Nb(2.6)	27.68	9.98	1:6.7
Nb(3.0)	18.20	10.98	1:11.1
Nb(4.3)	34.95	12.73	1:6.7
Ta(0.8)	32.98	5.37	1:3
Ta(2.5)	11.59	6.13	1:9.7
Ta(3.0)	10.45	7.13	1:12.6
Ta(3.8)	22.49	8.75	1:7.2
Ti(0.5)	46.44	7.57	1:3
Ti(2.5)	32.37	8.65	1:4.9
Ti(3.0)	18.17	10.99	1:11.2
Ti(4.1)	26.43	11.84	1:8.18

[a] The number in parentheses corresponds to the fulleride oxidation state as determined by Raman spectroscopy. For the Ti materials, these numbers were estimated according to the amount of added potassium and the XPS data because Raman measurements (Figure 3) revealed that these materials showed a mixture of fulleride oxidation states.

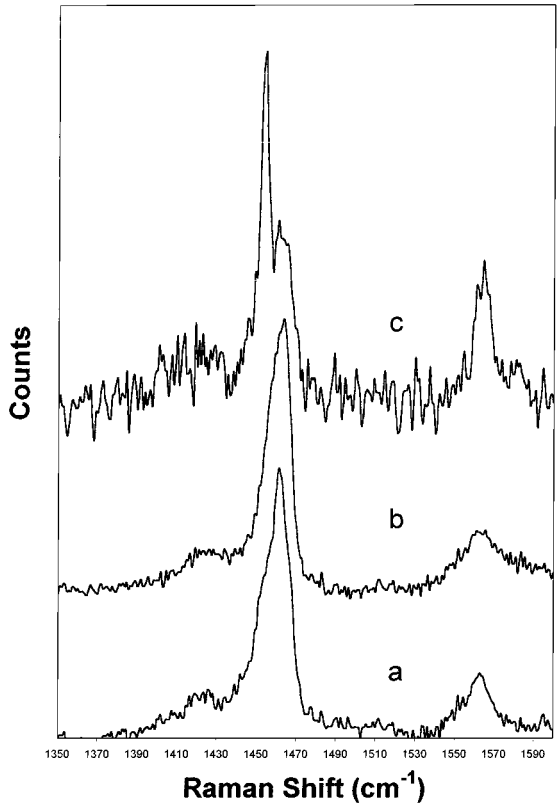

Figure 3. Raman spectra of the A_g region of samples of (a) large-pore mesoporous niobium oxide, (b) small-pore mesoporous tantalum oxide, and (c) small-pore mesoporous titanium oxide after treatment with excess K_3C_{60}.

hence, a higher level of retained fulleride. The Raman spectrum of this new composite (Figure 3a) shows strong absorbances at 1462 cm^{-1} (A_g) and 1422 cm^{-1}, indicating that the C_{60} units are present in an oxidation state of roughly $n = 0.5$. For fulleride salts of the type A_nC_{60} (A = K, Rb, Cs), the A_g mode shifts by roughly 6 cm^{-1} for every integer increment in the value of n.[38] The small shoulder observed in this spectrum occurs in a small number of the intercalates in this study and is attributable to slight inhomogeneities in these materials resulting from incomplete mixing due to diffusion bottlenecks

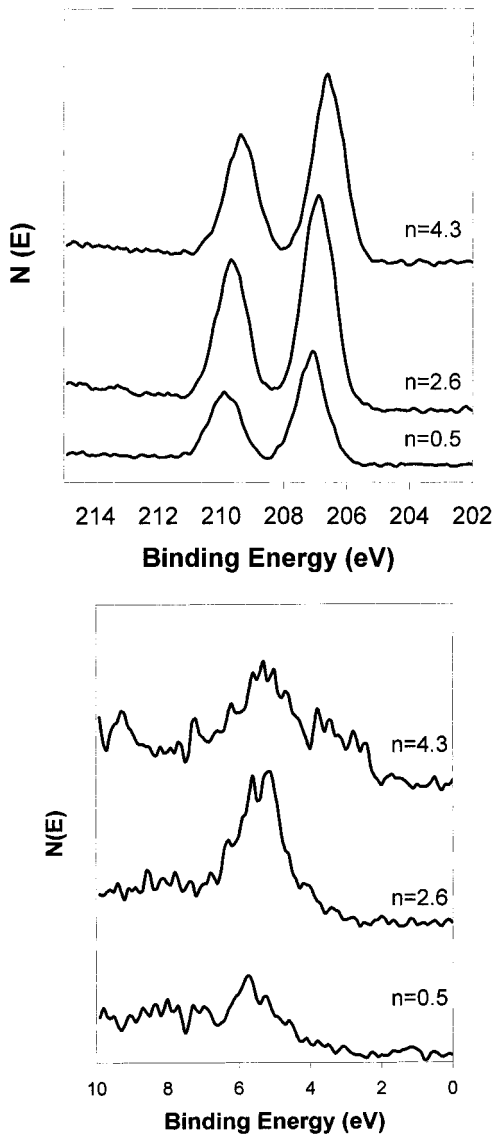

Figure 4. XPS spectra of (a) large-pore mesoporous niobium oxide samples treated with excess K_3C_{60} showing the Nb 3d $^5/_2$ and $^3/_2$ emissions for the parent intercalate and the materials reduced to $n = 2.6$ and $n = 4.3$ and (b) samples from a showing valence band region near the Fermi level.

in the pore structure. X-ray photoelectron spectroscopy (XPS) studies on this material (Figure 4a) displayed a niobium 3d $^5/_2$ emission at 207.1 eV, almost 1 eV lower than that of the parent mesoporous niobium oxide, which is consistent with reduction of the walls to an oxidation state of ca. 4.4^+, as compared to alkali metal reduced materials studied previously. In that independent study, it was shown that the Nb 3d $^5/_2$ and $^3/_2$ peak positions are sensitive to the degree of reduction of the walls of the mesostructure, as well as the nature of the countercation.[21] The distance to the Fermi level in the fulleride intercalate was roughly 4.0 eV (Figure 4b), similar to that observed in the XPS spectra of the material synthesized with 23-Å pores. The conductivity of samples of the potassium fulleride intercalate was measured by the four-point method under nitrogen and revealed that this material is a semiconductor, with a conductivity of $1.0 \times 10^{-3}\ \Omega^{-1}\ cm^{-1}$. This is almost identical to the value of $1.25 \times 10^{-3}\ \Omega^{-1}\ cm^{-1}$ obtained for the material synthesized with 23-Å pores. For

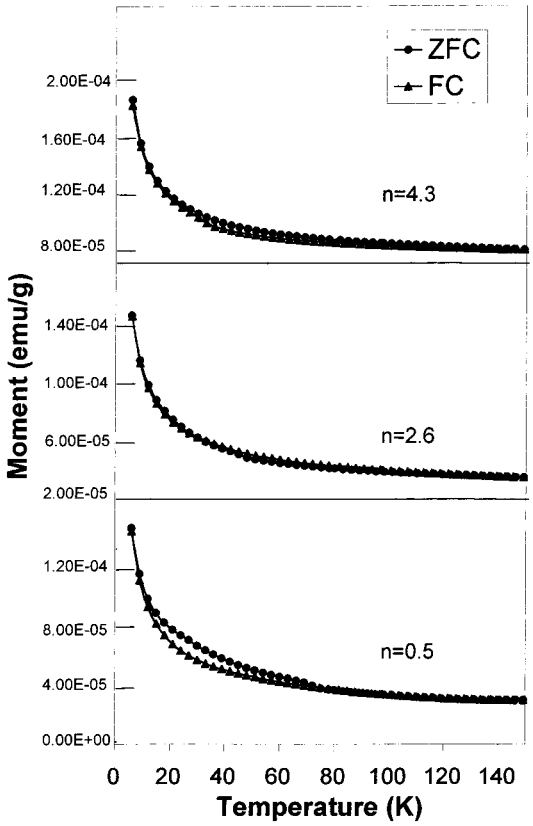

Figure 5. Plots of SQUID magnetization (emu) versus temperature for large-pore mesoporous niobium oxide treated with excess K_3C_{60}, as well as samples further reduced to $n = 2.6$ and $n = 4.3$

comparison, the room-temperature conductivity of K_3C_{60} measured by the four-point method is $0.58\ \Omega^{-1}cm^{-1}$ and that of K_1C_{60} is $1.93 \times 10^{-2}\ \Omega^{-1}cm^{-1}$. SQUID magnetic measurements conducted on this material over the temperature range of 4−100 K at 500 G demonstrated that the mesostructured intercalate is paramagnetic (Figure 5). The lack of superconductivity in these materials has been commented on before and can most readily be explained by the fact that the fulleride anion is in an oxidation state of $n = 0.5$, a state of reduction that shows no evidence of superconducting behavior. The electron spin resonance (ESR) spectrum of this material shows two peaks that are consistent with our previous observations in the material synthesized with 23-Å pores,[29] the broadest of which (line width = 35 G, $g = 2.003$) can be attributed to the t_{1u} electrons in potassium fulleride, as noted previously.[41] Because exchange interaction between localized spins will decrease with an increase in intermolecular distance,[42] the increase of the line width can be associated with a change in the spacing between fulleride units because of the confinement of the mesostructure. The narrow peak (line width = 2.0 G, $g = 2.003$) in this spectrum corresponds to the free electron in the mesostructure system, which is typically observed in our reduced mesoporous oxide.[20,23,29] These results are consistent with electronically isolated fulleride chains in the pores of a reduced paramagnetic host structure.

(41) Khaled, M. M.; Carlin, R. T.; Trulove, P. C.; Eaton, G. R.; Eaton, S. S. *J. Am. Chem. Soc.* **1994**, *116*, 3465.
(42) Bensebaa, F.; Xiang, B.; Kevan, L. *J. Phys. Chem.* **1992**, *96*, 10258.

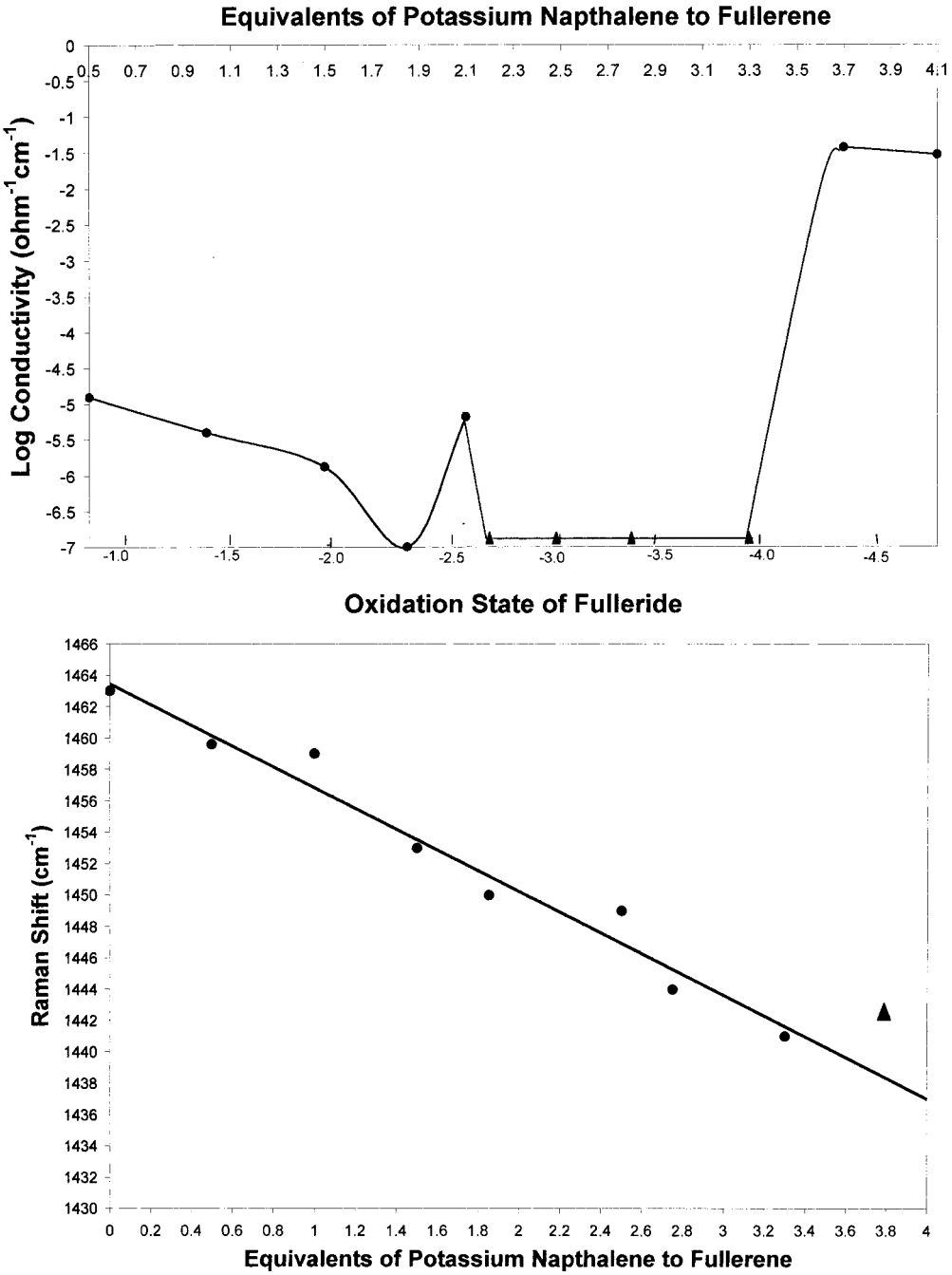

Figure 6. (a) Plot of oxidation state (error in $n = \pm 0.08$ units as calculated from the Raman shift) of intercalated fulleride in large-pore mesoporous niobium oxide versus logarithm of conductivity (estimated error = ±5%). The triangles represent areas in which the conductivity was lower than the range of our instrument. (b) Plot of Raman shift of A_g mode with increasing potassium content. The triangles represent deviations from linearity due to further reduction of wall structure.

To study the dependence of the conductivity and electronic behavior on the degree of fulleride reduction, the large-pore composite was titrated with potassium naphthalene. All materials retained their XRD patterns with a peak centered at 44 Å. The plot of oxidation state versus conductivity is shown in Figure 6a and exhibits distinct maxima at $n = 2.6$ and $n = 4.3$, very close to the pattern observed for the smaller-pore niobium oxide material studied previously. The plot of the Raman shift of the A_g band versus equivalents of potassium naphthalene added is also shown (Figure 6b) and displays a smooth linear progression, as previously observed for the reduction of the smaller-pore material, with a slight deviation from linearity at high levels of reduction. The materials at $n = 2.6$, 3.0, and 4.3 had carbon values of 27.68, 18.20, and 34.95%, respectively, with corresponding potassium values of 9.98, 10.98, and 12.73% (Table 1), showing a smooth rise with added potassium naphthalene. The decrease in the carbon content up to $n = 3$ is consistent with loss of fulleride from the channels as a result of increased Coulombic repulsion between fulleride units and increased potassium levels resulting from the high solubility of lower alkali fullerides in THF. The material at 4.3 shows a higher level of carbon because it is made directly from the parent intercalate and fullerides with higher alkali dopant levels are less soluble in THF. This might be because the potassium ions can diffuse into the pores and reduce the fulleride

more quickly than the fulleride can diffuse out of the pores, resulting in a trapping of insoluble fulleride units in the pores. This trend was also observed for the smaller-pore niobium oxide materials studied previously. The Nb 3d region of the XPS spectra for the materials at $n = 2.6$ and 4.3 is shown in Figure 4a and demonstrates that further reduction does not affect the oxidation state of the walls of the material until the $n = 4.3$ state, at which point the Nb 3d $^3/_2$ and $^5/_2$ peaks show signs of slight reduction to an average oxidation state of 4.2^+.[21] This is fully consistent with the Raman plot in Figure 6b, the deviation from linearity being caused by some of the reductant at this level being consumed by the walls rather than the fulleride. The presence of a broad emission from 2 to 3 eV in the Fermi region of the XPS spectrum of the $n = 4.3$ material (Figure 4b) in this sample is interesting, as conductivity in bulk fullerides is closely related to the density of states near the Fermi level[38] and metallic behavior in any material is normally marked by the presence of an electronic state tailing off into this region of lowest binding energy. The SQUID data are shown in Figure 5 and indicate that these materials are all paramagnetic, as observed for all previously studied fulleride intercalates. The magnetic moment increases with potassium loading as the level of unpaired electrons in the structure gradually increases. The ESR spectra of this series of materials exhibit a gradual merging of the peaks assigned to the walls of the mesostructure and the fulleride chain as the potassium loading level increases. This can be explained by the increasing of the exchange interaction as a result of the increase in the number of free electrons in the system. These observations are fully consistent with the ESR spectra of the composites synthesized from the smaller-pore Nb materials studied previously.[29]

Small-Pore Ta Materials. Whereas a change in pore size is expected to affect the electronic properties because of an increase in dimensionality, an increase in physical continuity, or an attenuation of possible lattice distortions due to the one-dimensional nature of the fulleride in the pores, changing the wall composition is expected to alter the electronic properties by changing the energy of the respective hybrid bands that might be involved in the conductivity of the composite. If conductivity of the $n = 4.1$ state is related to the electronic structure of the walls, this would most likely be due to an overlap of the Nb 4d or 5s (involved with the Nb−O sp conduction band) levels with the fulleride t_{1u} band. Because the population of the lower-lying 4d levels with up to 1 equiv of Na does not lead to conducting materials because of Anderson localization, it is likely that the involvement of the Nb−O sp conduction band and the t_{1u} band, and not the discontinuous Nb 4d band, are necessary in this transition at $n = 4.1$. Thus, with increased reduction of the material, the partially filled t_{1u} band of the fulleride unit must approach the requisite energy to overlap with this conduction band at and above a level of $n = 4.1$. Thus, a change from mesoporous niobium oxide to mesoporous tantalum oxide would result in a change from 5s to 6s and from 4d to 5d and a difference in energy of the sp conduction band. For this reason, a transition to metallic behavior involving an overlap with this band might occur at a different fulleride orbital energy level and, hence, a different degree of reduction.

When a sample of trimethylsilated Ta-TMS1 with an HK pore size of 22 Å, a BET surface area of 435 $m^2\ g^{-1}$, a pore volume of 0.213 $cm^3\ g^{-1}$, and an XRD peak centered at $d = 32$ Å is treated with excess K_3C_{60} for several days, followed by filtration and extensive washing, a new black material with a virtually identical XRD pattern (Figure 1b), a BET surface area of 161 $m^2\ g^{-1}$, an HK pore size of 19 Å, and a pore volume of 0.0875 $cm^3\ g^{-1}$ is formed. The nitrogen adsorption isotherm of this material is shown in Figure 2b. These data are consistent with retention of the mesostructure with concomitant absorption of K_3C_{60}. The Raman spectrum of this material confirmed the presence of fulleride with a strong peak at 1460 cm^{-1} (Figure 3b), corresponding to a fulleride oxidation state of $n = 0.8$. The change in oxidation state in the fulleride from $n = 3$ is expected considering the electron-accepting properties of the walls. The elemental analysis showed 32.98% C and 5.37% K with a molar C_{60}:K ratio of 1.0:3.0, as expected (Table 1). These values are in rough accord with the amounts of fulleride and potassium absorbed by the small-pore Nb system. The reduction of the Ta in the walls is reflected in the XPS of the Ta 4f $^7/_2$ and $^5/_2$ region (26.5 and 28.2 eV, respectively) shown in Figure 7a, which has shifted only slightly from that in the unreduced compound (26.9 and 28.7 eV), giving a mean oxidation state of 4.7^+ from comparisons with previous systems.[21] This is also consistent with previous work in our group that showed that the Ta materials are more difficult to reduce than the Nb materials. The valence region near the Fermi level is shown in Figure 7b and exhibits a broad hump for the Ta−O sp emissions tailing off at about 4.0 eV with very little closer to the Fermi level. SQUID magnetic measurements (Figure 8) show that this material is paramagnetic with no sign of a superconducting transition at 18 K as seen in pure K_3C_{60}. The ESR spectrum of this material is virtually identical to that of the large-pore Nb material, with overlapping broad and narrow peaks at ca. $g = 2.003$. The conductivity of this material was measured by the four-point method and found to be $9.9 \times 10^{-4}\ \Omega^{-1}\ cm^{-1}$, almost the same as observed for the Nb-based materials, indicating that the change in wall composition from Nb has little influence on the conductivity of the parent intercalalates.

To gauge the trend in conductivity with potassium loading, a series of alkali fulleride mesoporous tantalum oxide samples reduced with potassium naphthalene were prepared according to our previous procedure. These materials all showed complete retention of mesostructure as judged by the XRD pattern. As with the large-pore Nb system, the XPS spectra (Figure 7a and b) of the material of highest conductivity (in this case, at $n = 3.8$) showed evidence for a slight reduction of the mesostructure to a Ta oxidation state of 4.3^+, as evidenced by a move to lower binding energies in the Ta 4f $^5/_2$ and $^7/_2$ emissions while the emissions for the materials with lower levels of potassium remained unchanged. This material also had a smaller distance to the Fermi level (ca. 3.2 eV), fully supporting its increased conductivity. The SQUID data (Figure 8) showed that all materials were paramagnetic, with an

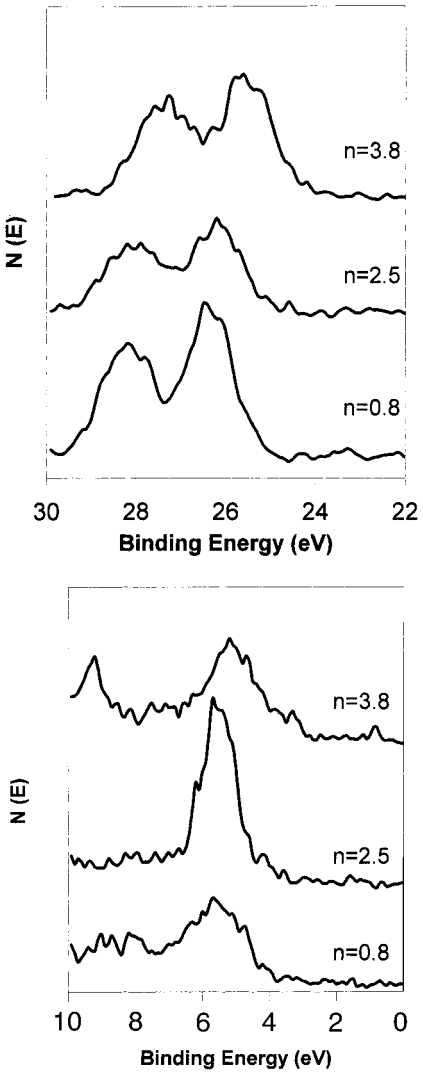

Figure 7. XPS spectra of (a) mesoporous tantalum oxide samples treated with excess K_3C_{60} showing the Ta 4f $^7/_2$ and $^5/_2$ emissions for the parent intercalate and the materials reduced to $n = 2.5$ and $n = 3.8$ and (b) samples from a showing valence band region near the Fermi level.

increase in magnetic moment with added potassium corresponding to an increase in unpaired electrons in the system. As with the Nb materials studied, the ESR spectrum showed a gradual merging of the two peaks for the free electrons in the wall and the fulleride phases, indicating a greater degree of electron exchange. Figure 9a shows a plot of the oxidation state of the intercalated fulleride, as measured by the position of the A_g Raman band, versus the logarithm of the conductivity. The maxima at $n = 2.5$ and $n = 3.8$ correspond to those in the niobium composite, but fall in slightly lower positions. The trend in the percentages of carbon and potassium at each of these maxima compares to those in the niobium composites (Table 1), with the K levels increasing with K loading and the C values dropping initially but then increasing again as the system approaches $n = 4$. Figure 9b shows a plot of Raman shift of the A_g band versus added potassium and exhibits a smooth linear progression as in the case of the Nb composites, but again with the deviation from linearity at high potassium levels expected from the slight over-reduction of the walls in this region.

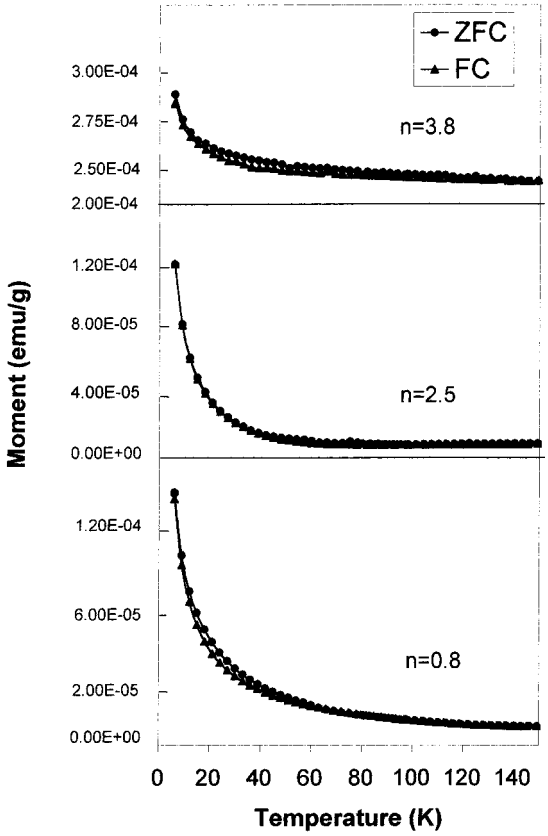

Figure 8. Plots of SQUID magnetization (emu) versus temperature for mesoporous tantalum oxide treated with excess K_3C_{60}, as well as samples reduced to $n = 2.5$ and $n = 3.8$.

Small-Pore Ti Materials. Changing the composition of the walls from Nb to Ta appears to have little effect on the pattern of double conductivity maxima, apart from a slight lowering of the K levels required for the transition to very high conductivity at 3.8 instead of 4.1. Because mesoporous titanium oxide undergoes an Anderson transition to higher conductivity and more continuous states with Li loading[21] (whereas mesoporous niobium and tantalum oxides do not), the mesoporous Ti system might exhibit different electronic behavior. When a sample of phosphate-free trimethylsilated Ti-TMS1 with an HK pore size of 25 Å, a BET surface area of 826 $m^2\ g^{-1}$, a pore volume of 0.486 $cm^3\ g^{-1}$, and a broad XRD peak centered at $d = 37$ Å is treated with excess K_3C_{60} in THF for several days, followed by filtration and extensive washing, a new dark brown material with no XRD pattern (Figure 1c) and a BET surface area of 325 $m^2\ g^{-1}$, an HK pore size of 23 Å, and a pore volume of 0.223 $cm^3\ g^{-1}$ is formed. The nitrogen adsorption isotherm of this material is shown in Figure 2c. These data are consistent with retention of the mesostructure without retention of long-range mesoscopic order on absorption of K_3C_{60}. All reduced mesoporous Ti materials studied previously lose their XRD pattern but maintain high surface areas and narrow pore size distributions. The Raman spectrum of this material shows a strong peak at 1462 cm^{-1} (Figure 3c) for the A_g band, indicating an oxidation state of the fulleride in the channels of $n = 0.5$, and a second band indicating that this material is not phase-pure, as in the case of the Nb and Ta composites. This might be due to a loss of mesoscopic order and partial structural

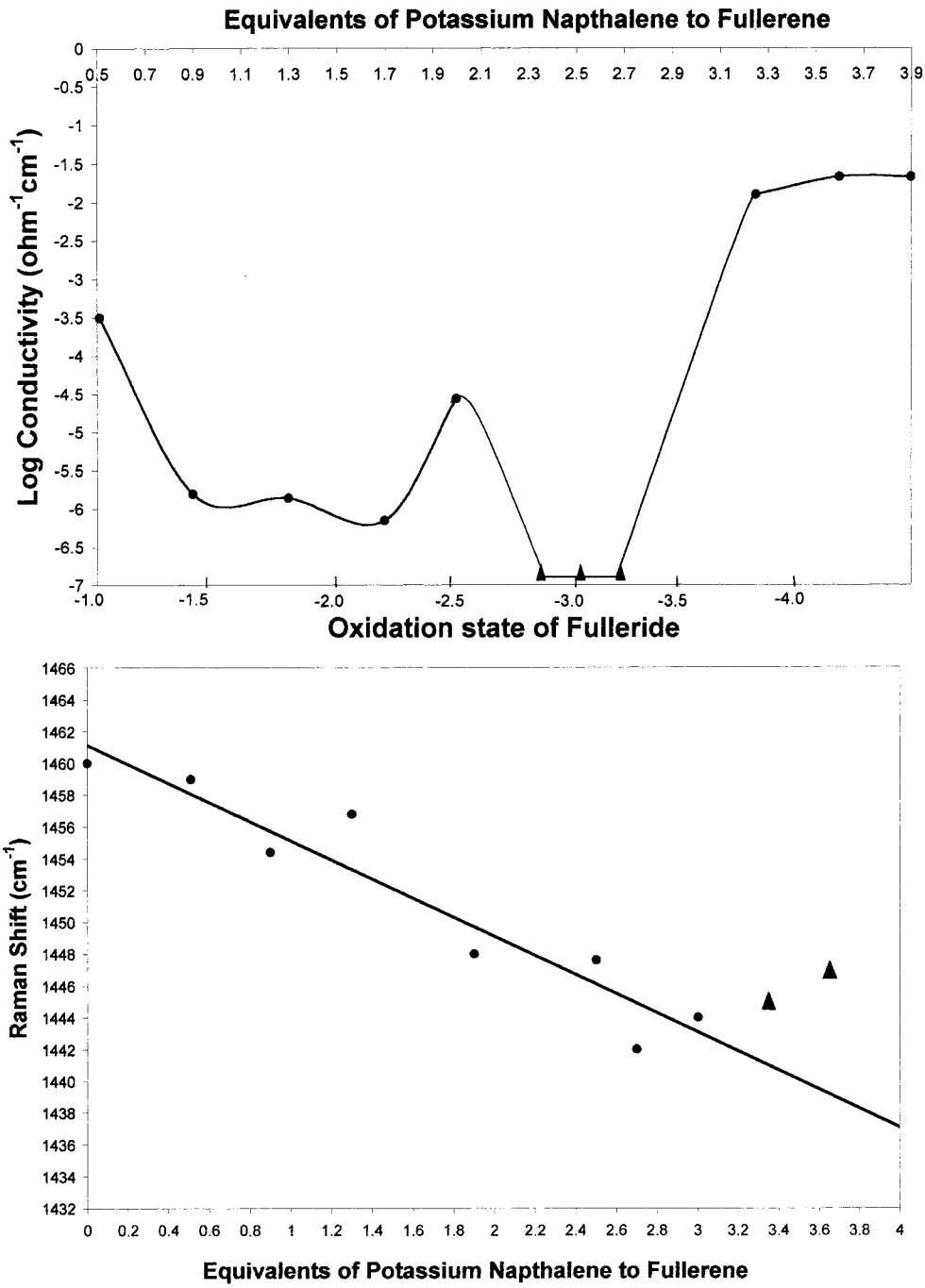

Figure 9. (a) Plot of oxidation state (error in $n = \pm 0.08$ units as calculated from the Raman shift) of intercalated fulleride in mesoporous tantalum oxide versus logarithm of conductivity (estimated error = ±5%). The triangles represent areas in which the conductivity was lower than the range of our instrument. (b) Plot of Raman shift of A_g mode with increasing potassium content. The triangles represent deviations from linearity due to further reduction of wall structure.

collapse, leading to a diffusion bottleneck that inhibits homogeneous distribution of the fulleride throughout the mesostructure. The reduction of the oxidation state of the fulleride to $n = 0.5$, however, confirms the transfer of an electron to the titanium oxide mesostructure. The elemental analysis shows that the material has absorbed 46.44% C and 7.57% K (Table 1), comparable to values for the small-pore niobium system, indicating, on the basis of the lower molecular weight of the titanium oxide versus niobium oxide, that the structure has actually absorbed less alkali fulleride, consistent with analogous cobaltocene composites of mesoporous titanium oxide, which absorb less cobaltocene than the corresponding niobium oxide materials. The XPS spectrum of the Ti 2p $^3/_2$ and $^1/_2$ region (458.3 and 463.8 eV, respectively) shown in Figure 10a has shifted with respect to that in the unreduced compound (459.3 and 464.9 eV) and corresponds to a mean oxidation state of Ti 3.7^+, demonstrating that the Ti materials are more difficult to reduce than their Nb counterparts.[21] The Ti−O sp valence region near the Fermi level is shown in Figure 10b and exhibits a large peak tailing off at about 3.0 eV as with the other parent intercalates in this study. The conductivity of this composite was measured to be 1.31×10^{-3} cm^{-1} Ω^{-1}, which compares with the values obtained for other composites accord-

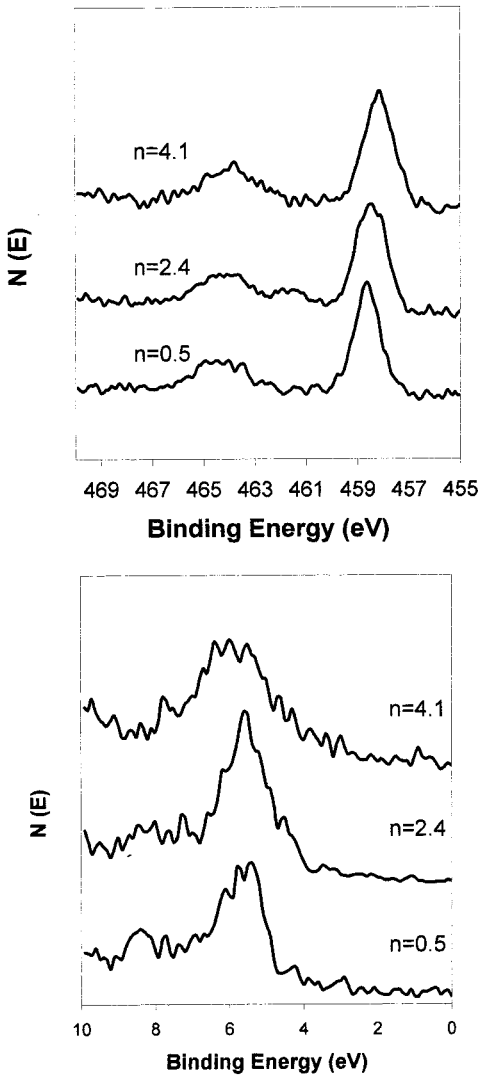

Figure 10. XPS spectra of (a) mesoporous titanium oxide samples treated with excess K_3C_{60} showing the Ti 2p $^3/_2$ and $^1/_2$ emissions for the parent intercalate, as well as the samples reduced to $n = 2.4$ and $n = 4.1$ and (b) samples from a showing valence band region near the Fermi level.

ingly. SQUID magnetic measurements (Figure 11) on this material show that it is paramagnetic with no sign of a superconducting transition. The ESR measurements revealed two overlapping peaks at ca. $g = 2.003$, one broad peak corresponding to the fulleride and one narrow peak corresponding to the free electron in the wall of the structure, almost identical to the spectra observed for other parent fulleride intercalates.

Despite the phase impurity of this material, stepwise reduction of the material was carried out in order to construct a plot of the logarithm of conductivity versus the degree of reduction in the material and revealed maxima at $n = 2.4$ and $n = 4.1$, as shown in Figure 12. These values were calculated on the basis of moles of K added per C_{60} and extrapolated according to the other plots, because the trend in change of Raman shift versus amount of potassium added did not follow a regular order, possibly as a result of quantum confinement effects on the energy of the symmetric A_g band associated with constricted pores resulting from the partial collapse of the mesostructure or the presence of two or more competing phases in the samples. Nevertheless,

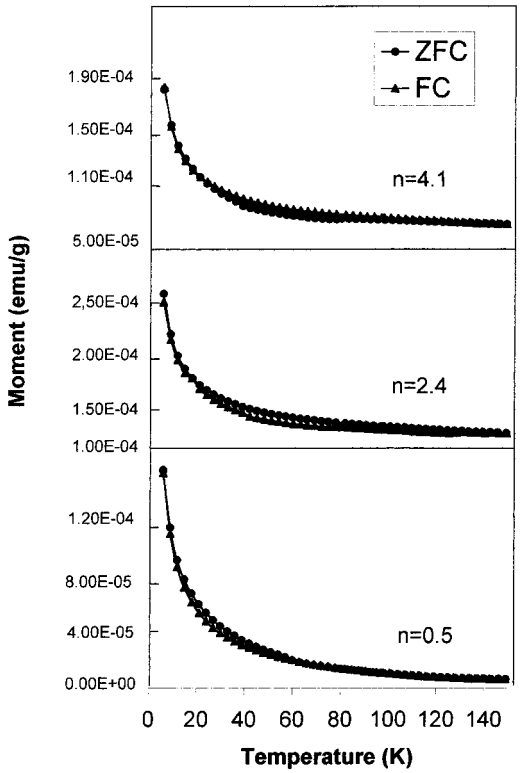

Figure 11. Plots of SQUID magnetization (emu) versus temperature for mesoporous titanium oxide samples treated with excess K_3C_{60} and reduced to $n = 2.4$ and $n = 4.1$.

the presence of these maxima compares closely with those in other materials studied in this series. The XRD data of materials in this series exhibited no peaks, whereas the nitrogen adsorption data showed evidence of residual mesoporosity expected from occluded disordered pores. As with the Ta materials, the XPS peaks showed little change on reduction for the materials at K levels below the transition to very high conductivity. Beyond this point, the Ti 2p $^3/_2$ and $^1/_2$ peaks shifted to slightly lower binding energy, consistent with reduction of the walls to a mean oxidation state of 3.3^+. In addition, the region near the Fermi level showed evidence of a greater density of states near the Fermi level, in accord with the Ta and Nb materials in this study. As with the other materials in this study, the SQUID plots showed standard Curie behavior with a general increase in magnetic moment with increase of reductant, consistent with a greater number of unpaired electrons in the structure. The ESR spectra mirrored those of the Ta and Nb systems in displaying a gradual merging of the two peaks for the fulleride and the walls of the mesostructure.

Discussion. In previous studies, we titrated a sample of a mesoporous niobium oxide−potassium fulleride composite with potassium naphthalene to establish the dependence of the conductivity on the oxidation state of the fulleride unit. The two surprising results were that there were two conductivity maxima, one at $n = 2.6$ and a second above $n = 4.1$. The maximum at 2.6 was linked to conductivity in bulk fullerides under the premise that, because of accidental vacancies in the crystal structure, the metallic phase was actually incrementally lower than $n = 3$, itself predicted to be a Mott−Hubbard insulator.[38] The maximum at $n = 4.1$ and higher cannot be directly related to bulk fullerides

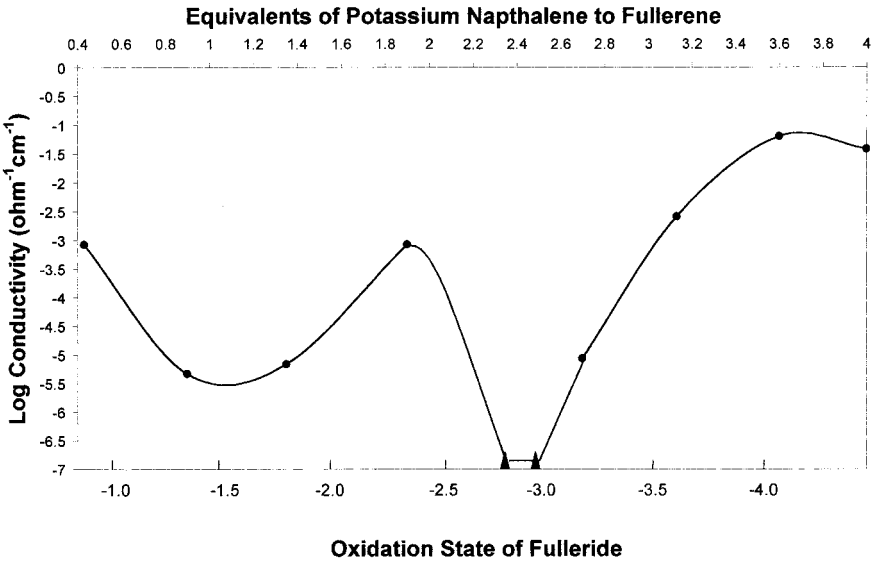

Figure 12. Plot of added potassium in mesoporous titanium oxide samples versus logarithm of conductivity (estimated error = ±5%). The triangles represent areas in which the conductivity was lower than the range of our instrument. The Raman spectra were not regular enough to assign definite oxidation states to the fulleride in any region.

or explained by conductivity in the walls of the mesostructure, as both K_4C_{60} and mesoporous niobium oxide reduced to a level comparable to that of the $n = 4.1$ composite are insulators. Results from the present study show that the double-maximum behavior is general and occurs in mesoporous tantalum oxide and mesoporous titanium oxide materials, as well as mesoporous niobium oxide materials with larger pores (22 Å as compared to 32 Å). While there appears to be some variation in the position of these maxima, the first always falls at or around $n = 2.5$ and the second falls at or around $n = 4.1$. There is also a trend in decreasing C content from the parent intercalate up to $n = 3.0$, after which the C content increases again. Because the amount of fulleride should have some effect on the conductivity, it seems logical to conclude that conductivity drops monotonically with C content, barring any special electronic states that might arise with reduction. Hence, the conductivity in all materials drops from that of the parent intercalate to $n = 2.4$ and then sharply rises at $n = 2.5$ or 2.6 as a result of the optimal loading of the t_{1u} band for electron mobility. The second maximum occurs universally at a C level that is higher than those of the materials at $n = 2.6$ and $n = 3.0$ but not as high as that of the parent intercalate. Thus, the 1000-fold increase in conductivity at this second maximum with respect to the parent intercalate cannot be accounted for by the fulleride loading level and must be related to an electronic transition in the material.

The first set of maxima can be related to the $n = 3$ state in bulk fullerides, occurring at a different position either because the one-dimensional phase has subtle one-dimensional distortions of the electron density or bandwidth that affect this parameter or because $n = 3$ is actually insulating, as predicted by Mott−Hubbard theory, and the $n = 2.5$ state is responsible for conductivity and present in bulk K_3C_{60} in the form of accidental vacancies. At this level, the ESR spectra strongly suggest that the fulleride phase and the reduced walls of the structure are acting as isolated electronic systems. The fact that Nb and Ta materials reduced to oxidation states between 4^+ and 5^+ by alkali naphthalene reagents are insulating suggests that all conductivity in these materials is related to electron mobility in the fulleride phase. This is thus an ideal system for studying the effects of reduction on isolated one-dimensional fulleride phases. The fact that changes in the pore size and the composition of the walls do not affect the position of this first maximum to a great extent agrees with this model, as the conductivity of an isolated fulleride nanowire should not be influenced by its surroundings.

Understanding the nature of the second maxima is more difficult. Although changes in energies of the d bands in the wall on going from 3d to 4d to 5d or variation in redox behavior might be important factors in determining the nature of this transition, there appeared to be little difference between the Nb, Ti, and Ta materials, all of them undergoing a transition to high conductivity at or around $n = 4$. Because the bulk $n = 4$ state is insulating and the alkali metal reduced materials at identical levels of mesostructure reduction (as judged by the XPS data) are also insulating, it suffices to say that this transition is likely related to a transition from isolated fulleride chains in the pores to cooperative behavior in which a hybrid t_{1u}−M *n*d or t_{1u}−MO sp CB (M = Nb, Ta, Ti) orbital is involved. The XPS data are certainly in accord with this picture, as all three materials in this study show an obvious increase in density of states near the Fermi level, supporting a transition to a more continuous and highly conductive state in which electron mobility between the fulleride phase and the walls of the structure is more facile. This picture is also supported by the gradual merging of the peaks in the ESR spectra upon reduction, a sign of increased electron mobility.

Conclusion

In conclusion, we have prepared a series of mesoporous transition metal oxide (M = Nb, Ti, Ta) composites with one-dimensional fulleride chains in the pore structure to study the dependence on pore size and wall composition of the conductivity patterns in the reduced

series between $n = 0.5$ and $n = 4.5$. These studies revealed that the double-maximum behavior is general and that the positions of the double maxima and the relative conductivities of the materials were comparable. Conductivity clearly depends on fulleride loading and decreases monotonically with decreasing percentage of carbon from $n = 0.5$ to $n = 2.0$. The transitions around $n = 4$ are related to an increased density of states near the Fermi level and increased cooperative behavior, most likely resulting from a more favorable overlap in the band structure of these composites. Efforts are ongoing to investigate the dependence of conductivity and physical behavior on the alkali metal and the absolute level of carbon in the pore structure with a view toward further elucidating the structural nature of the intercalated phase through solid-state NMR and EXAFS studies.

CM0104001